Journal of Electroanalytical Chemistry 966 (2024) 118399

Contents lists available at ScienceDirect

Journal of Electroanalytical Chemistry

journal homepage: www.elsevier.com/locate/jelechem

Studying ion transport dynamics in electrochemical measurements of lateral flow assays

Grégoire Le Brun [a,*], Enric Calucho [b,c], Margo Hauwaert [a], Ramy Moumneh [a], Gabriel Maroli [b,c], Sami Yunus [a], Giulio Rosati [b], Ruslan Álvarez-Diduk [b], Andrew Piper [b,*], Arben Merkoçi [b,d], Jean-Pierre Raskin [a]

[a] Institute of Information and Communication Technologies, Electronics and Applied Mathematics, UCLouvain, 1348 Louvain-la-Neuve, Belgium
[b] Nanobioelectronics & Biosensors Group, Institut Català de Nanociència i Nanotecnologia (ICN2), CSIC and the Barcelona Institute of Science and Technology (BIST), Campus UAB, 08193, Bellaterra, Barcelona, Spain
[c] Universitat Autònoma de Barcelona (UAB), Bellaterra, Barcelona, Spain
[d] Institució Catalana de Recerca i Estudis Avançats (ICREA), Passeig Lluís Companys 23, 08010 Barcelona, Spain

ARTICLE INFO

Keywords:
Lateral flow assays
Electrochemistry
Electrochemical impedance spectroscopy
Microfluidics
Ion transport
Point-of-care

ABSTRACT

Lateral Flow Assays (LFAs) are among the most widely used biosensors. Conventional colorimetric LFAs yield binary, non-quantifiable results. Electrochemical LFAs (eLFAs) aim to overcome this limitation. However, the reported disadvantage of extreme sensitivity to experimental conditions poses a significant challenge in the development of new eLFAs. In this work, impedimetric measurements were performed to probe the impact of experimental factors such as electrolyte conductivity/ionic strength on the eLFA outcomes. The time-dependent evolution of non-Faradaic impedance measurements coupled with flow velocity computations were employed to investigate ion transport across different LFA configurations and buffer compositions. The analysis of the Péclet number, a characteristic dimensionless parameter of flow dynamics within the LFA, revealed the coexistence of diffusive and convective ionic transport regimes over the LFA operational time. In addition, our findings underscore the critical role of absorbent pad dead volume adjustments in governing the capacity to maintain sample flow within the membrane over extended durations. These electro-fluidics phenomena are essential considerations for conducting electrochemical measurements within LFAs. Overall, this study offers insights into key design parameters for the integration of electrochemistry into LFAs.

1. Introduction

The LFA is a powerful point-of-care biosensing technology for the diagnosis of diseases [1]. They meet all the REASSURED criteria which are: Real-time connectivity, Ease of specimen collection, Affordable, Sensitive, Specific, User-friendly, Rapid and robust, Equipment-free or simple, and Deliverable to end-users [2]. The most widely used LFAs are colorimetric and fabricated out of fibrous materials such as glass wool or cellulose derivatives, e.g. nitrocellulose (NC) in the case of pregnancy self-tests or SARS-CoV-2 rapid tests. When a small volume of sample (typically microliters) is added to the test, it spontaneously flows along the strip, driven by capillary forces within the membrane. The detection of an analyte often relies on the formation of an immunoassay sandwich at the test line, which can be detected by the naked eye thanks to the accumulation of gold nanoparticles (AuNP), functionalised with specific bioreceptors [3]. To work properly, different phenomena occur at different time scales within the LFA: the flow of the components through the porous NC membrane, target-nanoparticle binding, and target-AuNP complex capture at the test line by immobilised bioreceptors, e.g. antibodies. The typical total time from sample introduction to test result takes 10–20 min. The development of a conventional colorimetric LFA involves the optimisation of these interconnected phenomena to achieve the highest test line intensity [3].

While colorimetric LFAs have shown sufficient performance for screening applications characterized by a qualitative and typically binary outcome, like pregnancy tests, their relatively low sensitivities and high limits of detection are inadequate for numerous other applications. In recent years, significant efforts have been focused on the development of new transduction mechanisms in LFA to improve their sensitivity and detection limits, taking advantage of the excellent physico-chemical

* Corresponding authors.
E-mail addresses: gregoire.lebrun@uclouvain.be (G. Le Brun), andrew.piper@icn2.cat (A. Piper).

https://doi.org/10.1016/j.jelechem.2024.118399
Received 22 March 2024; Received in revised form 21 May 2024; Accepted 31 May 2024
Available online 1 June 2024

properties of nanoparticles (fluorescence, electroactivity, magnetism, etc.) [4,5] or new LFA designs [7]. Among the available transduction modes, electrical transduction, specifically by measuring changes of dielectric properties of target analytes or nanoparticle labels accumulated at the test line, have already been widely explored [8]. The facile miniaturization of required instrumentation, coupled with the sensitive and quantitative detection achievable in such systems, renders electrochemical transduction an ideal means of enhancing sensing capabilities within LFAs, while enabling digitalization of the output at the point-of-care (PoC) [8,14,15].

The incorporation of electrochemical transducers onto LFA strips presents significant challenges, particularly in integrating electrodes for analyte sensing while ensuring robustness against the intrinsic variability across LFA components, encompassing structural materials to LFA buffers and flow. First, the design and fabrication process of the LFA must be engineered to accommodate electrodes and optimized for electrochemical measurements. For instance, Perju *et al.* have embedded electrodes directly within the LFA design by means of treating electrospun nanofibers, enabling flow-through and promoting interaction between the electrodes and the entire sample [9]. Despite recent methodological progresses for the introduction of reduced graphene oxide on nitrocellulose for eLFA development [11], the integration of unconventional compounds and fabrication techniques complicates the straightforward and cost-effective reel-to-reel assembly process of conventional LFAs [12].

A second challenge lies in understanding the electro-fluidic dynamics resulting from the spontaneous capillary forces within LFAs, which is crucial for optimizing eLFA sensing performance. Given the extreme sensitivity of electrochemical measurements to experimental conditions (ionic strength, pH, temperature), even minor sources of error are likely to be magnified in an eLFA if it is poorly understood and developed. Variations in fluid flow, e.g. due to membrane wetting, drying or material heterogeneity, as well as manual handling during sample deposition, can lead to significant discrepancies between LFA strips. This complexity in result interpretation poses challenges for eLFAs, necessitating robust analytical approaches to mitigate these effects [13,14]. In particular, the transport phenomena of highly conductive physiological buffers, such as phosphate buffered saline (PBS), and their supporting ions within the LFA needs to be analysed and controlled. Convection and diffusion have previously been noted to significantly impact electrical measurements in eLFAs by modifying the properties of the media at the electrode interface [14], yet they have scarcely been characterized for paper-based devices.

In conventional electrical paper-based analytical diagnostic devices (ePADs), flow injection analysis (FIA) is commonly utilized for diagnostics [10,16]. They involve the sequential injection of different reagents into the cellulose device to reveal target biomolecules at the detection zone. These devices incorporate specific designs with large fan-shaped collector pads at the far end of the strip, allowing each successive reagent to reach the reaction zone, thus ensuring sustained flow and delivery of samples and reagents over significantly longer periods than a simple paper strip. However, the multiple steps and reagents often complicate flow dynamics and signal interpretation. It is anticipated that this interpretation is further complicated in the case of FIA applied to eLFAs, where the multiple pads and interfaces significantly influence the capillary flow depending on their material properties and geometries.

These three challenges could be addressed with a better understanding of the flow dynamics on the transducer outcomes and how these devices could be engineered to improve performances. While eLFAs are a promising technology for PoC biodetection, this remains a major bottleneck as Perju and Wongkaew concluded in a topical review [8].

This work aims to investigate the challenges in integrating electrochemical measurements within LFAs by studying the electro-fluidic dynamics of the capillary flow within eLFAs. First, we engineered an eLFA design capable of non-Faradaic impedance measurements, which remains compatible with the conventional LFA manufacturing processes. A setup of external and reusable electrodes were positioned above and below the test and control lines in a custom-built cartridge (Fig. 1), in contrast with the typical electrodes integration in the literature, in which the electrodes are single use by virtue of their fabrication directly onto the paper-based devices [11,17–18]. Then, the mass transport regime within the LFA membrane was examined optically alongside continuous non-Faradaic impedance measurements of buffers with varying ionic strengths. The temporal evolution of the impedance signal highlights the different LFA microfluidic regimes and underscores the challenges in implementing FIA in conventional LFAs due to their limited absorbent pad capacity. Finally, design modifications to the LFA dead volume, combined with fluid velocity analysis, are proposed to investigate ionic transport dynamics within FIA measurement schemes over prolonged durations. This study advances the understanding of crucial features and considerations in integrating electrical transducers into LFAs, aiming to improve the interpretation of such measurements and accelerate progress towards the realization of practical eLFAs.

2. Materials and methods

2.1. Materials

Nitrocellulose membranes without a polyester backing (UniSart Lateral Flow CN140 unbacked, 8 μm nominal pore size, 140 μm thickness) were purchased from Sartorius (Göttingen, Germany). Cellulose membrane (CFSP001700) and glass fibre were purchased from Merck Millipore (Billerica, MA, USA). Supporting adhesive cards were purchased from Kenosha (Amstelveen, The Netherlands). Phosphate-buffered saline tablets (PBS 10 mM), sodium chloride solution (NaCl, 1 M) and silver conductive paste were purchased from Sigma-Aldrich (St. Louis, MO, USA). Deionized (DI) water was produced in our facilities (Millipore RX-75) followed by Millipore Super-Q (conductivity $\sigma = 5.56 \times 10^{-6}$ S/m at the output).

2.2. A plug-and-play, reusable cartridge integrating electrodes for impedance measurements within LFAs

Fig. 1(a) shows a schematic representation of the experimental system used to obtain impedance measurements in a LFA. In this design, the LFA is inserted into a cartridge designed specifically for the intended application. In this setup the working and counter electrodes are placed above and below the NC membrane to form parallel plates. This setup has been previously studied by our group [19]. The gold electrodes were fabricated by evaporating 500 nm of gold onto plastic support sheets (PET) using a physical vapour deposition (PVD) technique (ATC8E-Orion e-beam evaporator, AJA international). 2 mm × 15 mm electrodes were cut from the gold coated PET by hand. The electrodes were affixed to the cartridge with double-sided tape and could be reused up to 20 times before the mechanical degradation of the gold surface occurred due to abrasion upon contact with the LFA NC membrane. Conductive silver paste was applied onto the gold at the electrode extremities to enable the connection with the potentiostat probes. The cartridge was designed such that one or two pairs of electrodes can be placed on the LFA (2 × working electrodes, WE, and 2 × counter electrodes, CE) (Fig. 1(b)). For most of the impedance experiments, a single WE-CE pair is situated at the LFA test line (TL). For the specific experiment measuring ion transport velocity by impedance, a second electrode pair is integrated onto the distal portion of the NC membrane to constitute a control line (CL), positioned 9 mm apart from the TL, thereby establishing a differential measurement configuration. To obtain a visual confirmation of the proper capillary flow within the LFA, the NC membrane between the two electrode pairs is still visible through an aperture in the cartridge (Fig. 1(c)). The cartridge was 3D-printed in two pieces on an UltiMaker S3 (UltiMaker, NY, USA) using grey PLA

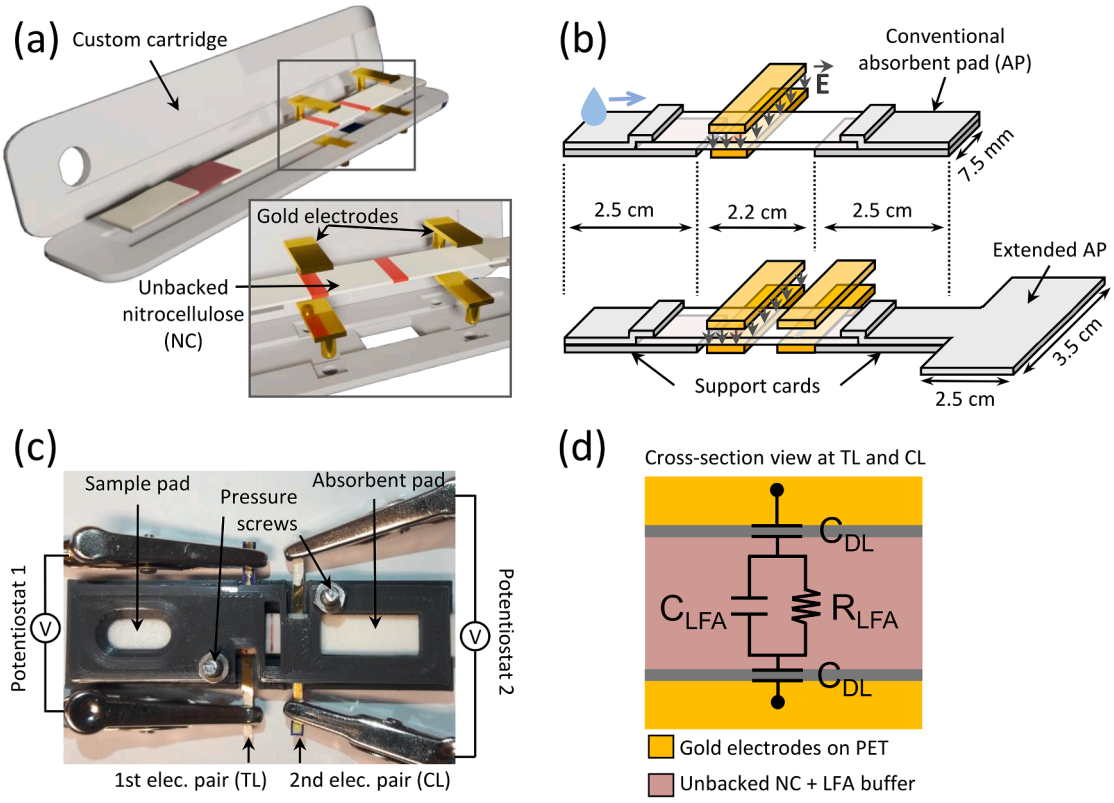

Fig. 1. (a) Schematic representation of the setup for non-Faradaic impedance measurements in LFAs. The colored test and control lines are shown to aid the reader in understanding the positions of the electrodes, but this study does not imply optical detection with gold nanoparticles. (b) Details of the eLFA formats explored in this study. (c) Photograph of the reusable, 3D-printed cartridge integrating two pairs of planar gold electrodes, each connected to an independent potentiostat. (d) Equivalent electrical model at the test and control lines of the eLFA used in this study, showing the two electrodes in gold, the nitrocellulose in mauve and the electrical double layer in grey.

filaments (Fig. S1.). A single cartridge was reused with new LFA strips for all the measurements in this article. The alignment and tightness between the WE, CE and the NC membrane, have to be precise and well-controlled to avoid poor measurement reproducibility (ensure good contact but not impede the solution flow in the membrane). Screws were added to the design to clamp both upper and lower parts of the cartridge and ensure homogeneous pressure and reproducible assembly around the LFA.

2.3. Fabrication of the lateral flow assays

Unbacked CN140 nitrocellulose membranes were adhered to laminated support cards. The cellulosic sample pad (SP) and absorbent pad (AP) were assembled on the laminated card overlapping the NC membrane by 2 mm. The cards were then cut into 7.5 mm-wide lateral flow strips with a strip cutter (KinBio, Shanghai, China). To expose the nitrocellulose, making it accessible to the electrode on the top and bottom of the membrane, a 2.2 cm wide opening was cut in the laminated support card, and the membrane was stuck on both sides of the support card to form a bridge between the sample pad and the absorbent pads sides. For the eLFA presenting an increased dead volume in this study, the absorbent pads made from cellulose sheets were enlarged (35 mm × 25 mm). The rectangular extension designed to fit with the LFA strip has the same length as the conventional absorbent pad (20 mm). (Fig. 1(b)).

2.4. Impedance parameters and sensor modelling

Impedance measurements in the presence of 150 μL of buffers with different conductivities were conducted at the TL location on conventional LFAs. The conductivity of the electrolyte solutions was measured using a benchtop conductivity meter (Conductivity Meter Sevencompact S230, Mettler-Toledo Ltd., UK). We used DI water and 10 mM PBS as upper and lower limits of our sample resistivities, respectively, since most environmental and PoC samples will have resistivities that lie between the two [19]. The different saline buffers compositions and electrical properties are detailed in Table 1. In accordance to previous works [19], an analytical model of the LFA test zones inserted in between the two gold electrodes is established to provide a physical understanding of the system. The equivalent electrical model (Fig. 1(d)) considers a double layer capacitance (C_{DL}) that establish at the metal-electrolyte interface due to charge redistribution occurring when solid materials are immersed in saline buffers. In these conditions, surface effects due to the double layer typically dominate at low frequencies (f < 10 kHz). The equivalent circuit also considers the NC membrane soaked with the saline buffers, modelled through the parallel association of its capacitive (C_{LFA}) and conductive (R_{LFA}) properties. Since the interface is non-Faradaic, there is no electron transfer. Therefore, there are no Warburg elements or charge transfer resistances like in the Randles' equivalent circuit [20].

2.5. Real-time impedance measurements on LFA, data analysis, and model fitting

The impedance measurements were performed by connecting each of the electrode pairs in the cartridge, through crocodile clips, either to a Metrohm AutoLab PGSTAT12 potentiostat with frequency response analyzer (FRA2) or to a Metrohm μSTAT Multi-4 multistat with 4

Table 1
Electrical Properties of various physiological buffers at 20 °C, utilized in LFA operations and investigated in this study for the response of the eLFA prototype. Variability in measured conductivities is attributed to practical errors during dilution.

Physiological buffer	Content	Measured conductivity σ (S/cm)	Description
Phosphate-buffered saline (PBS 10 mM)	PBS 10 mM (137 mM NaCl, 2.7 mM KCl, 10 mM Na_2HPO_4, 1.8 mM KH_2PO_4)	$\sim 1.55 \times 10^{-2}$	Main physiological buffer used in biological applications.
Conjugate Pad Buffer (CPB)	PBS 10 mM containing 5 % (wt/vol) sucrose, 1 % (wt/vol) BSA and 0.5 % (vol/vol) Tween-20	$[1.34–1.40] \times 10^{-2}$	Buffer used in the LFA conjugate pad to store the conjugated gold nanoparticles in colorimetric LFAs. It is imperative for the release and flow of AuNPs along the nitrocellulose strip after LFA rewetting.
PBS buffer diluted 10x (PBS 1 mM)	PBS buffers from the initial PBS 10 mM stock solution diluted in DI water.	$[1.50–1.70] \times 10^{-3}$	PBS dilutions are used to model the electrical properties of various real aqueous samples that could be loaded in LFAs. PBS 10 mM and DI water are considered as the upper and lower conductivity limits of the aqueous samples used in LFAs.
PBS buffer diluted 100x (PBS 100 μM)		$\sim 1.80 \times 10^{-4}$	
PBS buffer diluted 1000x (PBS 10 μM)		$[1.20–1.60] \times 10^{-5}$	
Deionized water (DI)		5.56×10^{-6}	Value refereed from our production facilities.

independent channels each with their own FRA modules (Metrohm, Utrecht, The Netherlands). ZVIEW software (Scribner Associates Inc., Southern Pines, NC, USA) was used to analyse the data by fitting to the appropriate equivalent circuit. Prior to each impedance measurement, an open-circuit and short-circuit calibration was performed to evaluate the impedance contribution of connections, ensuring proper device assembly and connection. Between each measurement, the reusable cartridge was opened, and the electrodes were washed with DI water. Between each measurement, the reusable cartridge was opened, and electrodes were cleansed with DI water. Subsequently, they were gently wiped using Kimtech cellulose wipes to prevent salt residue accumulation. Unless stated otherwise, all experiments were repeated five times (n = 5). However, in some figures, it has only been possible to show representative examples of the data.

To investigate the mass transport regimes of conventional LFAs, a cartridge with a single electrode pair located at TL was used to monitor the temporal evolution of LFA impedance following the addition of either DI water, 1 mM or 10 mM PBS (150 μL) to the LFA. Continuous impedance measurements were conducted for over 3 h during LFA operation at 100 kHz and 10 mV voltage amplitude. This was achieved by configuring custom NOVA and DropView procedures with the Autolab and μSTAT instruments, respectively.

To conduct continuous impedance analysis within the different LFAs formats, FIA experiments were performed. This involved injecting 50 μL of two different saline solutions sequentially, 10 mM PBS and 10 μM PBS, into the LFA sample pad every 15 min (Fig. 2). The nitrocellulose membrane was never allowed to dry, with more solution being added to the sample pad to keep it wet throughout. In the experiment involving the simultaneous analysis of impedance recorded by two electrode pairs from the cartridge, connected to independent channels of the μSTAT, the two impedance measurements were plotted on the same graph to determine the time delay required for charge transport along the NC membrane.

To address fabrication disparities among electrode pairs, primarily stemming from hand-cut geometries, as well as variations between LFAs and differences in pressure at the electrode-LFA interfaces, the analysis focused on a subset of measurements. Data was only excluded when it could be explained by one of these sources of error. Measurements from electrode pairs that exhibited poor interfacing with LFAs, as determined by noise and impedance amplitude assessment, were excluded. Continuous evaluation of measurement quality based on background noise characteristics (smooth or rough curves) facilitated the detection of any connection failures occurring during the measurement. Variability within and between functional electrode pairs was examined through statistical analysis, specifically mean and standard deviation calculations of impedance amplitude across different frequencies, depicted on Fig. S2 and Fig. S3 respectively, indicating the large influence of the

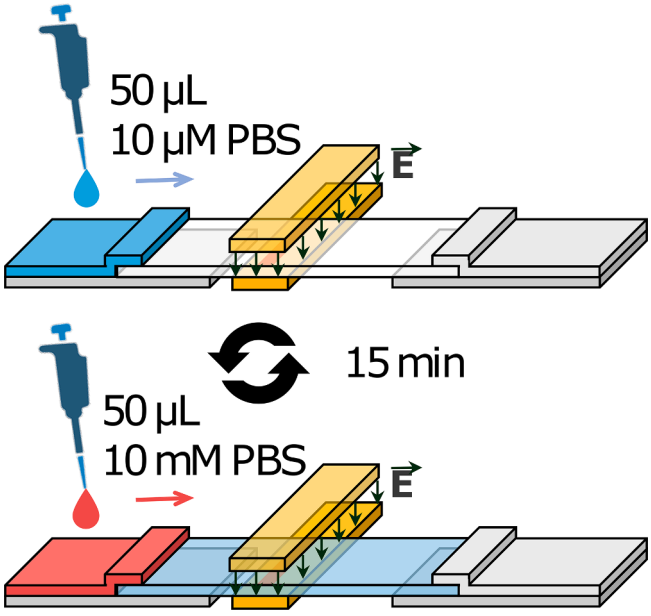

Fig. 2. Flow injection experiments coupled with impedance measurements were conducted following a protocol involving repeated, sequential injection of 50 μL of two distinct saline solutions (10 mM PBS and 10 μM PBS) at 15-minute intervals into the sample pad, spanning over a period exceeding 90 min. The depicted images show coloured samples for illustrative purposes only.

fabrication process and measurement protocol on the impedance recorded. Given the irreproducibility in electrode and LFA fabrication, it was difficult to directly compare the impedimetric responses of repeats. A major advantage of sequential injection analysis is that the device does not require prior calibration. Instead, by successive injection of buffers of known conductivity, it incorporates internal calibration and control measurements that effectively remove the detrimental analytical effects caused by device-to-device or reagent variations [16]. Therefore, when studying the mass transport with different saline buffers, we decided to only proceed with sequential injection analysis and compare impedimetric LFA measurements performed with the same cartridge and electrodes.

2.6. Colorimetric observation of the flow speed

To investigate the flow velocity of successively injected samples during flow injection impedance analysis, the temporal advancement of injections along an LFA strip was visualized. This was achieved by diluting blue and red pen inks (Pelikan) into 10 mM PBS and 10 μM PBS,

respectively. These coloured solutions were then sequentially injected into an LFA in accordance with the same temporal sequence as the PBS buffers during the flow injection impedance analysis. Their wicking within the membranes was recorded using an automated camera setup recording one image of the LFA every second, and the advancement of the coloured buffer front position was quantitatively assessed by an algorithm through image treatment.

3. Results

3.1. Implementation of a reusable cartridge and impedance spectroscopy parameters

The custom-based cartridge featuring one pair of electrodes at the TL was initially employed to determine the optimal frequency for impedance analysis of the saline buffers. Impedance measurements were conducted using frequency sweeps ranging from 1 MHz to 0.1 Hz on a conventional LFA strip immersed in saline buffers (Fig. S4). The impedance modulus significantly decreased with increasing frequency until reaching a plateau at 1–100 kHz depending on the buffer resistivity. Analysis of the impedance phases revealed that capacitances dominated at lower frequencies (f < 1 kHz). The capacitive behaviour was modelled as the double-layer capacitance (Fig. 1(d)); however, it should be noted that the electrodes are in contact with the nitrocellulose, making the nature of this capacitance complex. While this capacitance gives insights into the dielectric properties of the medium flowing through the NC, the swelling and solvation of the nitrocellulose during the wetting phase lead to changes in the contact area with the electrode surface, complicating the interpretation of capacitance measurement. For these reasons, our investigation focused on the solution resistance. At higher frequencies (f > 10 kHz), the capacitive elements have a minimal contribution to the measured impedance and only changes in the resistance of the LFA medium between the working and counter electrodes (R_{LFA}) dictates the total impedance through the saline buffer and NC membrane resistivities. To validate this hypothesis, we fitted the impedance measurements with the equivalent circuit for non-Faradaic systems and found that the fitted values for R_{LFA} were consistent within error with the impedance at 0.1 MHz of each of the PBS solutions tested (Fig. S5). Hence, changes in the resistance of the LFA medium are most accurately measured at high frequencies, for example by operating

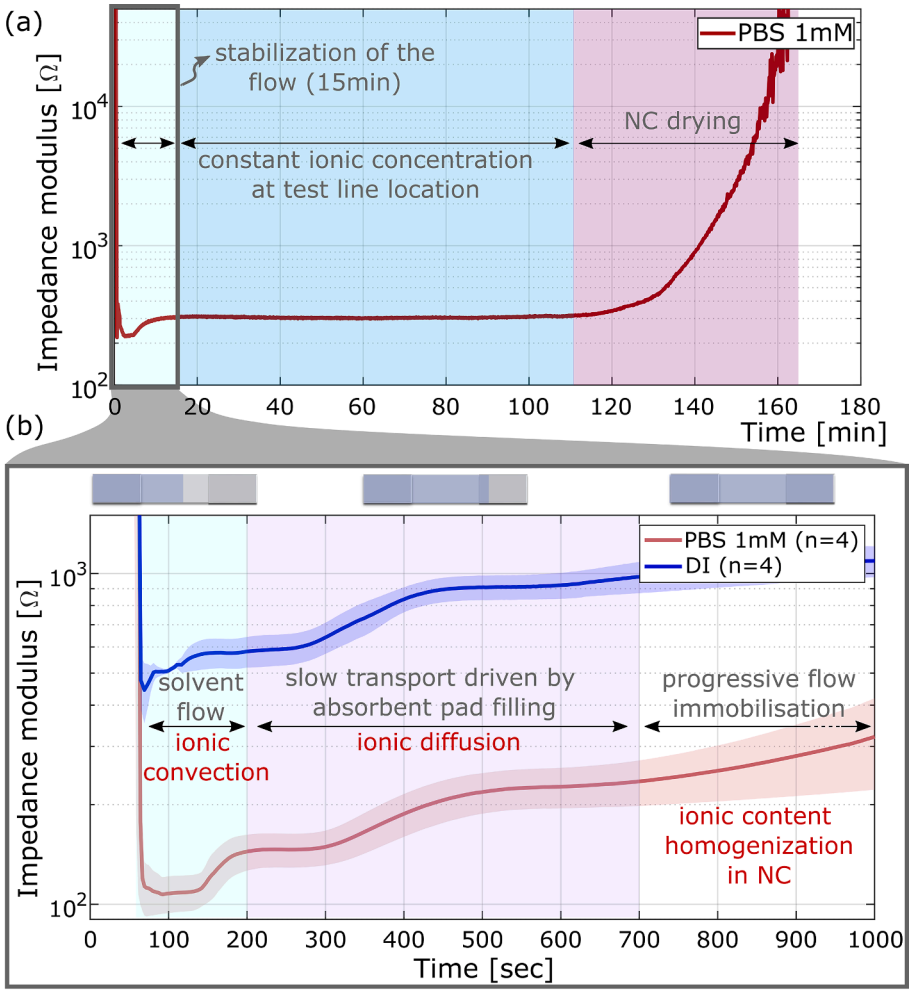

Fig. 3. (a) Representative impedance measurement obtained at the test line (TL) location during a drying study of a conventional LFA. The period from 15 min to approximately 110 min illustrates a consistent, stable ion concentration across the NC membrane, and therefore between the electrodes at the TL. The initial fluctuating impedance within the first 15 min underscores the time needed for LFA flow and subsequent ionic transport to stop. Following approximately 100 min, drying starts at the sample pad and absorbent pad, swiftly followed by NC membrane. (b) Various fluidic regimes were discerned when monitoring impedance over the course of LFA operation. For the first 100 s, the initial decrease in impedance can be attributed to enhanced ion transport, facilitated by fluid flow during the rapid mass transport regime initiated by wetting of the nitrocellulose membrane (solvent flow). Subsequently, impedance gradually increases towards stabilization, corresponding to the absorbent pad assuming control of fluidics within the strip. Once the absorbent pad is saturated, flow ceases (t > 700 *sec*), leading to an increase in impedance and homogenization of the ionic content within the membrane, ultimately achieving complete stabilization for times > 15 min. The blurred areas represent standard deviations.

the device at the fixed frequency of 0.1 MHz, as would be expected [21,22].

3.2. Time-resolved impedance measurements highlight different mass transport regimes in LFA

Subsequently, the two-electrode device, i.e. with a single electrode pair located at the TL, was employed to examine mass transport across conventional LFA strips during their standard operating duration, offering insights into the inherent electro-fluidic phenomena within the detection area. Typically, the investigation of mass and charge transport within LFAs is conducted empirically through colorimetric assays or liquid mass content analysis [23]. To the best of the authors' knowledge at the time of writing, the characterisation of such phenomena using non-Faradaic impedance measurements has not been previously reported.

We conducted impedance measurements over an extended duration (~3 h). The real-time impedance signal exhibited an initial fluctuation in ionic concentration at the test line location during the initial 15 min of LFA operation, with the effects of LFA drying becoming apparent after approximately 2 h (Fig. 3(a)). Consequently, for the conventional LFA format used in this study, there exists a 105-minute window wherein stable impedance measurements, and thus constant ionic concentration, can be observed in such eLFAs. The temporal evolution of the LFA impedance modulus within the initial 15 min following fluid injection was subsequently examined with increased temporal resolution (Fig. 3 (b)). Upon the arrival of the first fluid at the electrode area, an initial drop in impedance was observed after approximately 80 s. Following this, a brief period (lasting tens of seconds but varied with strip repeats) of stable modulus ensued, succeeded by two peaks in the modulus, indicating fluctuating ionic content within the flow over the course of LFA operation. These temporal observations agree with findings from previous studies, such as Gasperino et al. [23] which identified four fluidic regimes during LFA operation: (1) rapid flow during NC membrane wetting, (2) impregnation of the absorbent pad from the membrane, (3) filling of the absorbent pad, and (4) flow stops and progressive drying of the LFA via evaporation from the LFA sides.

To understand the origin of the initial impedance drop, we investigated the transport mechanism of the ions within the LFA flow at that particular moment. Mass transport of species in microfluidics is described by the Péclet number which compares convection versus diffusion rates and is defined by Eq. (1): [24]

$$P_e = V\frac{r_c}{D} \tag{1}$$

where V is the velocity of the fluids moving through the LFA membrane, r_C is the average size of the pores inside the membrane, and D is the diffusivity of the species transported in the fluids. The Pe value describes the transport mechanism: the mass transport of the species is convective if $Pe > 1$, and diffusive if $Pe < 1$.

To determine the velocity of the moving fluid optically, an automated camera setup was designed which enabled to record the advancement of the fluid front of coloured saline buffers over time during the first seconds of the LFA operation (Fig. S6(a-b)). This setup was used to prove that the impact of the pressure induced by the cartridge clamping screws on the flow rate within the eLFA was non-significant (Fig. S6(c)). These measurements showed a solvent flow velocity V of approximately 400 μm/s (2.4 cm/min) after the first 10 s of the LFA initiation, a figure in the same order of magnitude than flow rates previously reported in the literature for similar LFA and NC membranes [23]. The diffusion coefficient of NaCl, the most concentrated ions in PBS, D_{NaCl} is 1.61×10^{-9} m^2/s [25], and the mean pore size of the NC membrane $r_C \simeq 7.5$ μm (as quoted by the manufacturer). The calculated Péclet number is approximately 1.8, indicating that ion transport in the LFA is primarily governed by convection. In other words, the rate of convection induced by capillarity exceeds the rate of diffusion. This rapid initial fluid transport implies rapid ionic mass transfer between the electrodes, potentially explaining the low impedances observed during this phase of the LFA operation. After stabilization, the flow velocity decreases. However, quantifying it using the image-based method is challenging due to the entire NC membrane being wet, rendering it impossible to accurately compute the flow velocity based on the optical contrast between the filled and unfilled regions. In accordance with Equation (1), a decrease in fluid velocity V corresponds to a reduction in the Péclet number. Based on flow rates previously reported in literature [23], the computed Pe is lower than unity, indicating diffusive ionic transport within the LFA flow. To summarise, we observed a faster convectional flow of ions when the solution was flowing through the NC membrane alone, impacting the measured impedance. However, by the time the absorbent pad started to wet, the flow rate had decreased to the point that a diffusion-controlled regime has been established.

3.3. Flow injection impedance analysis reveals sample homogenisation in conventional LFA

The diffusion of ionic species occurring during the absorbent pad-controlled fluidic regime raises questions regarding the feasibility of implementing FIA within conventional LFA devices. This entails successive reagents reaching the TL through prolonged temporal flow. To explore species mass transport within the NC, we continuously monitored impedance response at the TL while conducting a FIA experiment, sequentially adding 50 μL of buffers with different resistivities, specifically 10 mM and 10 μM PBS.

In the conventional LFA design, temporal impedance curves at 100 kHz exhibited notable changes upon the three first buffer injections, as expected (Fig. 4(a)). However, despite utilising an absorbent pad composed of a thick cellulose membrane, the impedance response (impedance peaks) could not be consistently reproduced upon repeated buffer injections starting from the second injection of PBS 10 μM. Specifically, the process failed to undergo multiple cycles of buffer injections due to the gradual reduction in fluid flow as the liquid-filled region of the LFA increased, resulting in viscous forces outweighing capillary forces and halting capillary flow once the total sample volume exceeded the strip dead volume. Beyond 50 min, the diminishing flow rate facilitated ion diffusion from regions of higher concentration (PBS 10 mM) to those of lower concentration (PBS 10 μM) within the membrane, according to Fick's law, leading to a loss of control over ionic transport within the LFA. This was further investigated and validated by simulating the experiments colorimetrically using red and blue dyes instead of the various PBS concentrations (Fig. 4(b)), confirming the mixing of the buffers after 3 injections. As noted by Pradela-Filho *et al.* for continuous-flow electrochemical paper-based devices, this non-steady flow rate behaviour, leading to a progressive dilution of the samples, could be undesirable as it may affect both signal and reproducibility for specific detection setups, reducing accuracy and limiting applicability [10].

3.4. Enabling prolonged FIA measurements in eLFAs with expanded AP

To address the challenge of dilution observed upon repeated injections in conventional LFAs, an enlarged absorbent pad (AP) was incorporated into the eLFA design, substantially increasing the strip dead volume. Using continuous impedance measurements similar to those for conventional LFAs, the extended-AP LFA enabled the differentiation of multiple successive injections of PBS samples within the same strip (Fig. 5(a)). The experiment maintained identical injection volumes and time periods as previously, as they represent typical parameters for FIA applications in diagnostics within such LFA systems. The extended AP unsaturated region ensures a continuous buffer flow over 120 min, sustaining significant capillary forces to accommodate a higher sample load in the device, as modelled by Mendez et al. [6]

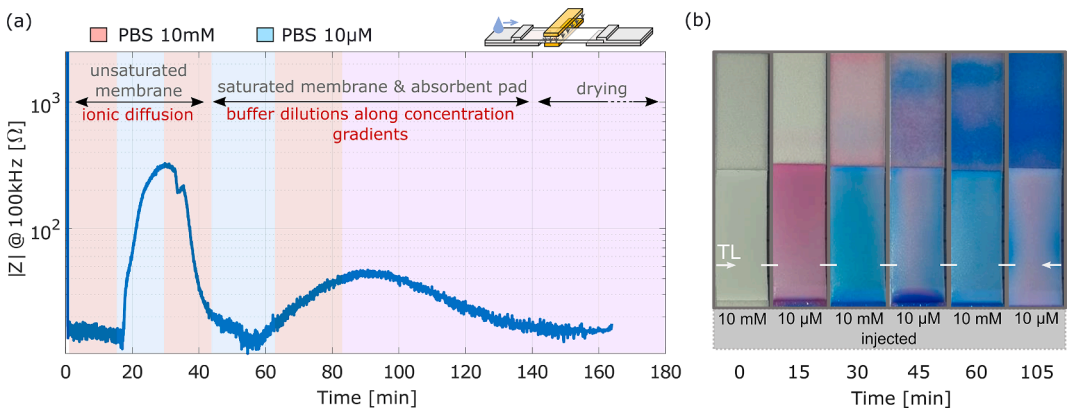

Fig. 4. (a) Typical flow injection impedance analysis of 50 µL of PBS 10 mM and 10 µM buffers in a conventional LFA design. Red and blue frames depict successive buffer injections of 10 mM and 10 µM PBS, respectively. Purple area represents homogenisation and dilution of the buffers in the membrane. During the first three injections, the impedance response of the conventional LFA varied with buffer conductivity as expected, after which it fell apart. This failure of the system with more injections was attributed to saturation of the LFA nitrocellulose and absorbent pad bed volumes. (b) The simulation of the successive injection of 50 µL of PBS 10 mM and PBS 10 µM with red and blue dyes highlights mixing of the buffers at 45 and 105 min, consistent with the impedance measurements. Therefore, a conventional LFA is not suitable for precise control of the ionic content within the LFA membrane. White stripes depict where the electrodes were placed in the eLFA set-up.

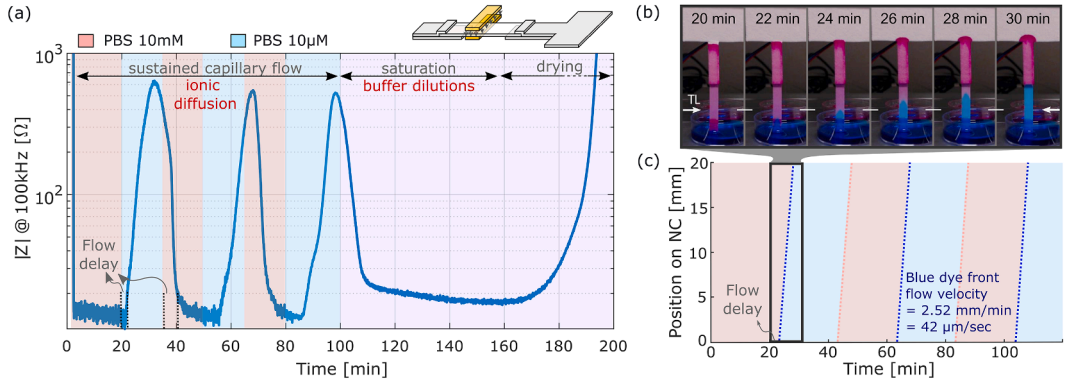

Fig. 5. (a) Typical impedance measurement data at 100 kHz of sequential flow injections of different salt buffers in a LFA with a large dead volume (extended absorbent pad). The sustained capillary flow in the unsaturated LFA facilitates the transport of sample buffers within the strip to the TL for extended periods, depicted by the repeated cycling with PBS buffers. Once the LFA dead volume reaches saturation (>120 min), the flow stops and is followed by progressive dilution of buffers within the strip. (b) Colorimetric simulation of the front flow interface progress between PBS 10 mM (with red dye) and PBS 10 µm (blue dye) by repeated cycles of flowing blue and red coloured buffers. (c) Position of the coloured flow on the NC membrane. The automated camera setup coupled to an image analysis algorithm depicted the repeated advancement of the front interfaces over the different PBS cycles (dashed diagonal lines). Strikingly, there is a consistent front flow velocity observed throughout the eLFA operation. The reduced velocity compared to the solvent flow is attributed to increased viscous forces encountered by the flow as it progresses through the AP.

(Fig. S6(d)). To determine the flow velocity within the eLFA during successive injections, impedance measurements were conducted using a cartridge with a differential measurement configuration, i.e., integrating two electrode pairs. Hence, the front flow velocity of the injected buffers was computed by comparing the time elapsed for an impedance change to occur between the TL and CL, which are positioned at controlled distances from each other. (Fig. S7). These findings were compared with flow velocities deduced from colorimetric experiments employing extended AP (Fig. 5(b-c)). Constant flow velocities throughout the eLFA operation were computed to be 2.7 mm/min and through the colorimetric tests were calculated as 2.52 mm/min. Indeed, once the flow reached the AP, its velocity was no longer dictated by the initial solvent flow rate (NC wetting), but by the flow in the AP, which is slower due to increased viscous forces. This led to a change in the constant flow rate in the NC strip without buffer mixing [6,26], confirmed by colorimetric experiments where the fronts are distinctly observed without apparent mixing of dye. A flow velocity of 2.6 mm/min, the average of the two measured flow velocities, results in a Péclet number of approximately 0.2. This value suggests that ion transport in the LFA during successive injections is primarily governed by diffusion. Notably, the constant flow velocity was sustained over approximately two hours. As long as the AP remains unsaturated, sustained capillary flow prevents dilution of ionic species between samples injected into the eLFA. However, the effect of the ionic diffusion within the flow is illustrated in Fig. 5(a) by the flow delay, representing the time required for the solution to reach the electrode TL. This flow delay becomes significant from the second injection.

4. Discussion

The objective of this study was to study ion transport mechanisms within LFAs with different AP geometries. Our findings suggest that capillary force driven wicking dominates when the flow passes solely through the NC. However, diffusion dominates once the solvent front reaches the absorbent pad, as the increased viscous force lowers the flow rate below the ion diffusion rate. Low solution resistances were observed during the initial fluid transport, attributed to the increased electrolyte concentration at the solvent front. Our results also demonstrate that generating a constant flow velocity over a long period of time can be achieved by increasing the dead volume of the AP, allowing for repeated

injection and migration of sample volumes typically used in LFAs (~100 μL). It is expected that modifying the flow velocity could be possible by adjusting the capillarity of the AP and the geometry (length) of the rectangular connection between it and the NC [6].

Secondly, the modular electrode cartridge allows for the easy addition of additional electrode pairs, which could facilitate multiplexed detection and mapping of processes within the LFA strips. This could also be used to catch faulty devices and reduce errors in electrochemical measurements, a matter of paramount importance in the deployment of LFAs for practical applications [27]. The use of a two-electrode setup limits the electrochemical measurements available. The system would be vastly improved by the ability to incorporate a formal reference electrode into the cassette, although this step has already presented practical difficulties due to the nature of LFAs. This is the focus of our ongoing research. In addition, the adoption of a reusable cassette and electrode configuration instead of a single-use design improves the sustainability of eLFA devices. It has been shown that a major part of the environmental impact of the production of electrochemical paper-based sensors is generated by the manufacturing process of metal electrodes, notably gold deposition [28]. Ensuring the effectiveness of electrode reuse requires the development of cleaning protocols during the sensor design phase, especially for sensors involving affinity reactions at the electrodes or the detection of pathogenic targets. Such cleaning methodologies have been proposed in prior studies [29].

Finally, the concept of flow control has been explored in paper-based microfluidic applications to ensure a steady-flow or constant supply of reactive species at the test line/control line [30–31]. Various publications have suggested modifying the geometry of paper-based devices to create fan shapes at the end, thereby increasing the dead volume and compensating for the increased viscous forces at the test area [6–7]. Recent studies of ePADs have employed this approach for continuous flow electrochemical detection of biomolecules [10]. However, this concept has not yet been fully integrated into commercial LFA designs, partly due to scalability issues arising from the current manufacturing process (cutting or deposition of hydrophobic barriers). Theories and models precisely describing the influence of LFA design parameters on continuous flow, including the geometry of pads and the interfaces between porous materials, are lacking. While this study provides initial empirical results, formalizing theoretical models precisely describing the electro-fluidic behavior of LFAs would aid in the design of more complex eLFAs and could improve sensor performance. For now, to guide the design of such eLFAs, we suggest calculating dimensionless numbers that characterize mass transport within the membranes, such as the Péclet number [24].

5. Conclusions

In this work, we present a study of the ionic transport dynamics within LFA flows to facilitate the implementation of controllable and reproducible electrochemical measurements in LFAs. We established a reusable setup employing two gold electrodes positioned above and below an unbacked nitrocellulose membrane to conduct impedimetric measurements within an LFA. Then, we systematically examined the ionic flow through the membrane by impedance. To assess the dominating transport mechanism (diffusion or convection) within different LFA designs, the Péclet number was computed based on flow velocity measurements, both from impedance and optical readouts. Our findings indicated that convection dominates when the flow is just through the NC, whereas diffusion becomes dominant once the solvent front reaches the absorbent pad. It is thus advisable to conduct electrochemical measurements in LFAs after the solvent front has reached the absorbent pad to obtain stable measurements. Finally, we demonstrated that flow injection analysis can be performed on LFAs, provided that the absorbent pad is sufficiently large to sustain the increasing viscous forces associated with the eLFA design and accommodate the total volume of solution added without surpassing the strip dead volume. These continuous flow injection experiments also highlighted the setup sensitivity to buffer changes, suggesting their potential in sensing applications.

Although electrochemical detection in LFAs presents attractive features such as high sensitivity, selectivity, low instrumentation cost, inherently quantifiable outputs, and improved analytical performance, the complexity of integration is often underestimated. Designing an electrical LFA necessitates a systematic approach to understanding the impact of all components and designs. Hopefully, by investigating and elucidating mass transport in eLFAs, this study will guide the future development of performing LFAs with electrical transducers.

CRediT authorship contribution statement

Grégoire Le Brun: Writing – review & editing, Writing – original draft, Visualization, Validation, Resources, Project administration, Methodology, Investigation, Funding acquisition, Formal analysis, Data curation, Conceptualization. **Enric Calucho:** Writing – review & editing, Investigation, Data curation. **Margo Hauwaert:** Writing – review & editing, Methodology, Investigation. **Ramy Moumneh:** Writing – review & editing, Investigation, Data curation. **Gabriel Maroli:** Writing – review & editing, Data curation, Conceptualization. **Sami Yunus:** Writing – review & editing, Investigation, Data curation. **Giulio Rosati:** Writing – review & editing. **Ruslan Álvarez-Diduk:** Supervision, Conceptualization. **Andrew Piper:** Writing – review & editing, Writing – original draft, Supervision, Methodology, Formal analysis. **Arben Merkoçi:** Writing – review & editing, Resources, Project administration, Funding acquisition. **Jean-Pierre Raskin:** Writing – review & editing, Supervision, Project administration, Funding acquisition, Conceptualization.

Declaration of competing interest

The authors declare that they have no known competing financial interests or personal relationships that could have appeared to influence the work reported in this paper.

Acknowledgments

The work of G. Le Brun, M. Hauwaert and R. Moumneh was supported by the FRIA-FNRS. G. Le Brun benefited from a travel grant from Wallonie-Bruxelles International. The work of S. Yunus was supported by Région Wallonne through the Win2Wal research program. The authors thanks N. Moreau for the 3D images. G. Maroli would like to express his gratitude to the Carolina Foundation for financial support through the scholarship "Doctorado 2020." G. Maroli acknowledges Universitat Autònoma de Barcelona (UAB) for the possibility of performing this work inside the framework of Chemistry PhD Programme. E. Calucho acknowledges Ministerio de Ciencia e Innovación of Spain and Fondo Social Europeo for the Fellowship PRE2018-084856 awarded under the call "Ayudas para contratos predoctorales para la formación de doctors, Subprograma Estatal de Formación del Programa Estatal de Promoción del Talento y su Empleabilidad en I + D + i", under the framework of "Plan Estatal de Investigación Científica y Técnica y de Innovación 2017-2020". E. Calucho also expresses his gratitude to Universitat Autònoma de Barcelona (UAB) for the possibility of performing this work inside the framework of Biotechnology PhD Programme.

Appendix A. Supplementary data

Supplementary data to this article can be found online at https://doi.org/10.1016/j.jelechem.2024.118399.

References

[1] J. Budd, B.S. Miller, N.E. Weckman, D. Cherkaoui, D. Huang, A.T. Decruz, N. Fongwen, G.-R. Han, M. Broto, C.S. Estcourt, J. Gibbs, D. Pillay, P. Sonnenberg, R. Meurant, M.R. Thomas, N. Keegan, M.M. Stevens, E. Nastouli, E.J. Topol, A. M. Johnson, M. Shahmanesh, A. Ozcan, J.J. Collins, M. Fernandez Suarez, B. Rodriguez, R.W. Peeling, R.A. McKendry, Lateral flow test engineering and lessons learned from COVID-19, Nature Rev. Bioeng. 1 (1) (2023) 13–31.

[2] K.J. Land, D.I. Boeras, X.-S. Chen, A.R. Ramsay, R.W. Peeling, REASSURED diagnostics to inform disease control strategies, strengthen health systems and improve patient outcomes, Nat. Microbiol. 4 (1) (2019) 46–54.

[3] C. Parolo, A. Sena-Torralba, J.F. Bergua, E. Calucho, C. Fuentes-Chust, L. Hu, L. Rivas, R. Álvarez-Diduk, E.P. Nguyen, S. Cinti, D. Quesada-González, A. Merkoçi, Tutorial: design and fabrication of nanoparticle-based lateral-flow immunoassays, Nat. Protoc. 15 (12) (2020) 3788–3816.

[4] V.-T. Nguyen, S. Song, S. Park, C. Joo, Recent advances in high-sensitivity detection methods for paper-based lateral-flow assay, Biosens. Bioelectron. 152 (2020) 112015.

[5] A. Sena-Torralba, R. Álvarez-Diduk, C. Parolo, A. Piper, A. Merkoçi, Toward Next Generation Lateral Flow Assays: Integration of Nanomaterials, Chem. Rev. 122 (18) (2022) 14881–14910.

[6] S. Mendez, E.M. Fenton, G.R. Gallegos, D.N. Petsev, S.S. Sibbett, H.A. Stone, Y. Zhang, G.P. López, Imbibition in Porous Membranes of Complex Shape: Quasi-stationary Flow in Thin Rectangular Segments, Langmuir 26 (2) (2010) 1380–1385.

[7] S. Kasetsirikul, M.J.A. Shiddiky, N.-T. Nguyen, Challenges and perspectives in the development of paper-based lateral flow assays, Microfluid. Nanofluid. 24 (2) (2020) 17.

[8] A. Perju, N. Wongkaew, Integrating high-performing electrochemical transducers in lateral flow assay, Anal. Bioanal. Chem. 413 (22) (2021) 5535–5549.

[9] A. Perju, F. Holzhausen, A.-M. Lauerer, N. Wongkaew, A.J. Baeumner, Flow-Through Carbon Nanofiber-Based Transducer for Inline Electrochemical Detection in Paper-Based Analytical Devices, ACS Appl. Mater. Interfaces 15 (38) (2023) 44641–44653.

[10] L.A. Pradela-Filho, E. Noviana, D.A.G. Araújo, R.M. Takeuchi, A.L. Santos, C. S. Henry, Rapid Analysis in Continuous-Flow Electrochemical Paper-Based Analytical Devices, ACS Sensors 5 (1) (2020) 274–281.

[11] E. Calucho, R. Álvarez-Diduk, A. Piper, M. Rossetti, T.K. Nevanen, A. Merkoçi, Reduced graphene oxide electrodes meet lateral flow assays: A promising path to advanced point-of-care diagnostics, Biosens. Bioelectron. 258 (2024) 116315.

[12] M. Baharfar, M. Rahbar, M. Tajik, G. Liu, Engineering strategies for enhancing the performance of electrochemical paper-based analytical devices, Biosens. Bioelectron. 167 (2020) 112506.

[13] C. Bathany, J.-R. Han, K. Abi-Samra, S. Takayama, Y.-K. Cho, An electrochemical-sensor system for real-time flow measurements in porous materials, Biosens. Bioelectron. 70 (2015) 115–121.

[14] L.J.K. Weiß, P. Rinklin, B. Thakur, E. Music, H. Url, I. Kopic, D. Hoven, M. Banzet, T. von Trotha, D. Mayer, B. Wolfrum, Prototype Digital Lateral Flow Sensor Using Impact Electrochemistry in a Competitive Binding Assay, ACS Sensors 7 (7) (2022) 1967–1976.

[15] L.A. Pradela-Filho, W.B. Veloso, I.V.S. Arantes, J.L.M. Gongoni, D.M. de Farias, D. A.G. Araujo, T.R.L.C. Paixão, Paper-based analytical devices for point-of-need applications, Microchim. Acta 190 (5) (2023) 179.

[16] L. Bezinge, Niklas Tappauf, D.A. Richards, C.-J. Shih, A.J. de Mello, Rapid electrochemical flow analysis of urinary creatinine on paper: unleashing the potential of two-electrode detection, ACS Sens. 8 (10) (2023) 3964–3972.

[17] L. Gonzalez-Macia, Y. Li, K. Zhang, E. Nunez-Bajo, G. Barandun, Y. Cotur, T. Asfour, S. Olenik, P. Coatsworth, J. Herrington, F. Güder, NFC-enabled potentiostat and nitrocellulose-based metal electrodes for electrochemical lateral flow assay, Biosens. Bioelectron. 251 (2024) 116124.

[18] A. Miglione, A. Raucci, F. Cristiano, M. Mancini, V. Gioia, A. Frugis, S. Cinti, Paper-based 2D configuration for the electrochemical and facile detection of paracetamol in wastewaters, Electrochim. Acta 488 (2024) 144255.

[19] G. Le Brun, M. Hauwaert, A. Leprince, K. Glinel, J. Mahillon, J.-P. Raskin, Electrical Characterization of Cellulose-Based Membranes towards Pathogen Detection in Water, Biosensors 11 (2) (2021) 57.

[20] A. Hassibi, R. Navid, R.W. Dutton, T.H. Lee, Comprehensive study of noise processes in electrode electrolyte interfaces, J. Appl. Phys. 96 (2) (2004) 1074–1082.

[21] N. Pal, S. Sharma, S. Gupta, Sensitive and rapid detection of pathogenic bacteria in small volumes using impedance spectroscopy technique, Biosens. Bioelectron. 77 (2016) 270–276.

[22] G. Brom-Verheijden, M. Goedbloed, M. Zevenbergen, A. Microfabricated, 4-Electrode Conductivity Sensor with Enhanced Range, Proceedings 2 (2018) 797.

[23] D. Gasperino, T. Baughman, H.V. Hsieh, D. Bell, B.H. Weigl, Improving Lateral Flow Assay Performance Using Computational Modeling, Annu. Rev. Anal. Chem. 11 (1) (2018) 219–244.

[24] Y. Liu, L. Zhan, Z. Qin, J. Sackrison, J.C. Bischof, Ultrasensitive and Highly Specific Lateral Flow Assays for Point-of-Care Diagnosis, ACS Nano 15 (3) (2021) 3593–3611.

[25] V. Vitagliano, P.A. Lyons, Diffusion Coefficients for Aqueous Solutions of Sodium Chloride and Barium Chloride, J. Am. Chem. Soc. 78 (8) (1956) 1549–1552.

[26] E.W. Washburn, The Dynamics of Capillary Flow, Phys. Rev. 17 (3) (1921) 273–283.

[27] M. Colombo, L. Bezinge, A. Rocha Tapia, C.-J. Shih, A.J. De Mello, D.A. Richards, Real-time, smartphone-based processing of lateral flow assays for early failure detection and rapid testing workflows, Sens. Diagn. 2 (1) (2023) 100–110.

[28] G. Le Brun, J.-P. Raskin, Material and manufacturing process selection for electronics eco-design: Case study on paper-based water quality sensors, Procedia CIRP 90 (2020) 344–349.

[29] J. Aleman, T. Kilic, L.S. Mille, S.R. Shin, Y.S. Zhang, Microfluidic integration of regeneratable electrochemical affinity-based biosensors for continual monitoring of organ-on-a-chip devices, Nat. Protoc. 16 (5) (2021) 2564–2593.

[30] J.A. Adkins, E. Noviana, C.S. Henry, Development of a Quasi-Steady Flow Electrochemical Paper-Based Analytical Device, Anal. Chem. 88 (21) (2016) 10639–10647.

[31] R.B. Channon, Y. Yang, K.M. Feibelman, B.J. Geiss, D.S. Dandy, C.S. Henry, Development of an Electrochemical Paper-Based Analytical Device for Trace Detection of Virus Particles, Anal. Chem. 90 (12) (2018) 7777–7783.